Behaviorally irrelevant feature matching increases neural and behavioral working memory readout: Support for activity-silent working memory

Aytaç Karabay[12], Michael J. Wolff[34], Veera Ruuskanen[1], & Elkan G. Akyürek[1]

[1] Department of Psychology, Experimental Psychology, University of Groningen, Groningen, The Netherlands

[2] Department of Psychology, Science Division, New York University Abu Dhabi, Abu Dhabi, United Arab Emirates

[3] Department of Experimental Psychology, University of Oxford, Oxford, United Kingdom

[4] Ernst Strüngmann Institute (ESI) for Neuroscience in Cooperation with Max Planck Society, Frankfurt, Germany

Running head: Visual impulse perturbation of working memory

Date: 1/23/2024

Word count: 8215

Address correspondence to:

Aytaç Karabay, Psychology Department, New York University Abu Dhabi

Saadiyat Island, New York University Campus, Abu Dhabi, United Arab Emirates

Email: a.karabay@nyu.edu

Abstract

The activity-silent framework of working memory (WM) posits that the neural activity during object perception and encoding leaves behind patterned, “activity-silent” neural traces that enable WM maintenance without the need for continuous, memory-specific neural activity. The presence of such traces in the memory network subsequently patterns its responses to external stimulation, which can be used to readout the contents of WM using an impulse perturbation or “pinging” approach. The extent to which the neural impulse response is patterned by the WM network should be modulated by the physical overlap between the initial memory item and the subsequent external perturbation stimulus, with higher overlap increasing WM readout. Here we tested this prediction in a delayed orientation match-to-sample task, by either matching or mismatching task-irrelevant spatial frequencies between memory items and impulse stimuli, and between memory items and probes. Matching frequencies resulted in faster behavioral response times, and increased the WM-specificity of the neural impulse response as measured from the EEG signal. We found no evidence that matching spatial frequencies resulted in globally stronger or different neural responses, but rather in distinct neural activation patterns. The beneficial effects of feature matching in our task support the tenets of the activity-silent framework of WM, and confirm that impulse perturbation interacts directly with the representations that are held in memory.

Keywords: working memory; impulse perturbation; EEG; multivariate pattern analysis

Cognitive neuroscientists attempt to relate cognitive processes to neural activity that is highly complex and multidimensional. Compounding this challenge is the fact that neural activity is only part of the picture. Synaptic processes that alter the functional connectivity in the brain's networks also play an important role. Such processes need not correlate strongly with neural firing, which makes them difficult to assess with non-invasive measurements. These difficulties have recently come to a head in the study of working memory (WM), where a debate has arisen about its neural basis (e.g., Masse et al., 2020; Sreenivasan et al., 2014).

Maintenance of information in WM was long thought to involve persistent neural firing, based on evidence of ongoing neuronal spiking during memory maintenance in higher-order cortex, including prefrontal and parietal areas (Curtis & D'Esposito, 2003; Funahashi et al., 1989). However, it has been suggested that this apparent "persistence" may be an artefact of trial averaging and temporal smoothing of short-lived oscillatory activity bursts interrupted by activity-silent periods (Lundqvist et al., 2016; 2018; Miller et al., 2018). These silent periods may be bridged via changes in synaptic efficacy (Kozachkov et al., 2022; Mongillo et al., 2008; Stokes, 2015). Specifically, during the encoding stage, the neural response to the sensory input leaves behind a patterned "silent" neural trace which supports WM maintenance (Stokes, 2015). This trace in turn patterns spontaneous neural activity (Sugase-Miyamoto et al., 2008), and can be read out by internally generated activity states (Lewis-Peacock et al., 2012; Sprague et al., 2016), or via the context-dependent neural response to external stimulation (i.e., 'pinging the brain': Stokes et al., 2013; Wolff et al., 2015; 2017). This may not necessarily be specific to WM, but could be a more fundamental property of dynamic network changes, resulting in distinct neural response profiles to subsequent input (i.e., dynamic coding: Stokes, 2015; Remington et al., 2018; see also Nikolić et al., 2009; Sugase-Miyamoto et al., 2008).

The pinging method involves presenting an invariant, task-irrelevant impulse stimulus (or alternatively, a TMS pulse; Rose et al., 2016) during the WM delay, while a participant's electroencephalogram (EEG) is recorded (Wolff et al., 2015; 2017). The impulse is thought to work analogously to sonar; as a surge of activation is driven through the network, the resulting pattern of activity reflects not only the invariant neural response to the impulse stimulus, but also the current state of the perturbed network. Given that the impulse response has been found to contain information about the contents of WM in various studies (e.g., Duncan et al., 2023; Kandemir & Akyürek, 2023; Wolff et al., 2015), this strongly suggests there is overlap between the network that responds to the impulse stimulus, and the network that contains WM-specific neural traces. Indeed, it has been found that while the neural impulse response to auditory stimulation during an auditory WM task contained information about the auditory WM content, using the same auditory stimulation in a visual WM task did not result in a WM-specific neural response (Wolff et al., 2020b). This implies that the neural impulse response is WM-specific as long as the neural processing of the impulse stimulus interacts with the sensory-specific WM trace, which should be more likely when WM memoranda and impulse stimulus share sensory modalities or other features.[1]

However, an alternative account has been put forward (Barbosa et al., 2021), which suggests that the primary effect of the visual impulse is to improve the signal-to-noise ratio (SNR) of ongoing neural activity (but see Wolff et al., 2021). If this is indeed the only function of the impulse, it would mean that the impulse does not actually perturb the memory network,

[1] Wolff et al., 2020b also showed that auditory WM representations can be perturbed by both auditory and visual impulses. This may however suggest that auditory information was visualized in their task. Furthermore, the modality-matching (i.e., auditory) impulse perturbed auditory representations better than the visual impulse, which is in line with our hypothesis.

but reveals items that are held in activity patterns hidden in noise, rather than activity-silent representations.

Providing evidence for “activity-silent” neural states during the WM delay is not straightforward with conventional neuroimaging techniques. While the decoding of WM content from delay activity states have been shown to essentially reach chance-level when attention is directed away (e.g., Wolff et al., 2017; Lewis-Peacock et al., 2012; Sprague et al., 2016; Watanabe & Funahashi, 2014), it can always be argued that the measurement tools are simply not sensitive enough to pick up the weak persistent activity that is nonetheless still present (Schneegans & Bays, 2017; Barbosa et al., 2021). On the other hand, as alluded to above, it can even be argued that persistence delay activity is an artefact of trial averaging (Lundqvist et al., 2016). Thus, to avoid these methodological shortcomings, in this study we focus on the dynamic signal evoked by the impulse stimulus, using an analysis method that is exclusively sensitive to dynamic signals, isolating the neural impulse response from possible stable activity states in EEG (Wolff et al., 2020), and examining how it is affected by task-irrelevant feature matching.

In our experiment, to assess to what degree the impulse response reflects a WM network-specific response, or alternatively, a global neural response (Barbosa et al., 2021), we used two different visual impulse and probe stimuli in a delayed match-to-sample task. The memory items were orientation gratings, and participants were asked to judge whether their orientation was clockwise or counterclockwise (CW, CCW) relative to that of a probe stimulus, which was presented after a short delay at the end of each trial. Critically, the impulses and probes either matched or did not match the memory items on their spatial frequency, which was an integral, but task-irrelevant feature (Fig 1a-b). Behavioral and neural findings suggest that objects are held in WM with all of their features (Lin et al., 2021; Luck & Vogel, 1997), even when some are

irrelevant (such as location: Zhou et al., 2022). This is in line with the activity-silent account of WM, where any stimulation leaves behind an initial neural trace, whether relevant or not (Mongillo et al., 2008; Nikolic et al., 2009; Stokes, 2015).

This suggests that the same orientations may be represented within distinct neural traces in WM if their task-irrelevant features are different. Based on this assumption, we hypothesized that if the impulse response reflects the perturbed WM network, as suggested by Wolff and colleagues (2017), a matching impulse should act like a matched filter and reveal the memory content with greater decoding accuracy because it targets the network storing the representation more precisely (Figure 1c). Similarly, a matching probe should improve behavioral readout by facilitating the transition towards the behaviorally relevant matched filter response (Myers et al., 2015; Stokes, 2015; Remington et al., 2018; Nikolic et al., 2009; Sugase-Miyamoto et al., 2008). However, there should be no effects of impulse spatial frequency matching, if the previously reported WM-specificity of the impulse response is not due to a targeted perturbation of a WM-specific neural trace, but rather due to stimulus-induced, global neural noise reduction which may facilitate the decodability of an active neural code (Barbosa et al., 2021; see also Churchland et al., 2010; Pfurtscheller et al., 1979; 1994), for example via phase reset (Wolff et al., 2021).

To preview the results, we show that a matching impulse produced better decoding of mnemonic representations from the impulse-evoked multivariate EEG pattern than a mismatching impulse, and that a matching probe reduced reaction times during memory recall. The stimulus-specific nature of the impulse response supports the idea that WM contents can be targeted directly by external perturbation, as predicted by the activity-silent WM framework (Stokes, 2015; Wolff et al., 2017). The positive behavioral effect of matching probes further

suggests that the specificity of the impulse response is unlikely to be an epiphenomenon, but may rather reflect WM coding that is optimal for the task at hand (cf. Myers, 2022; Nairne, 2002).

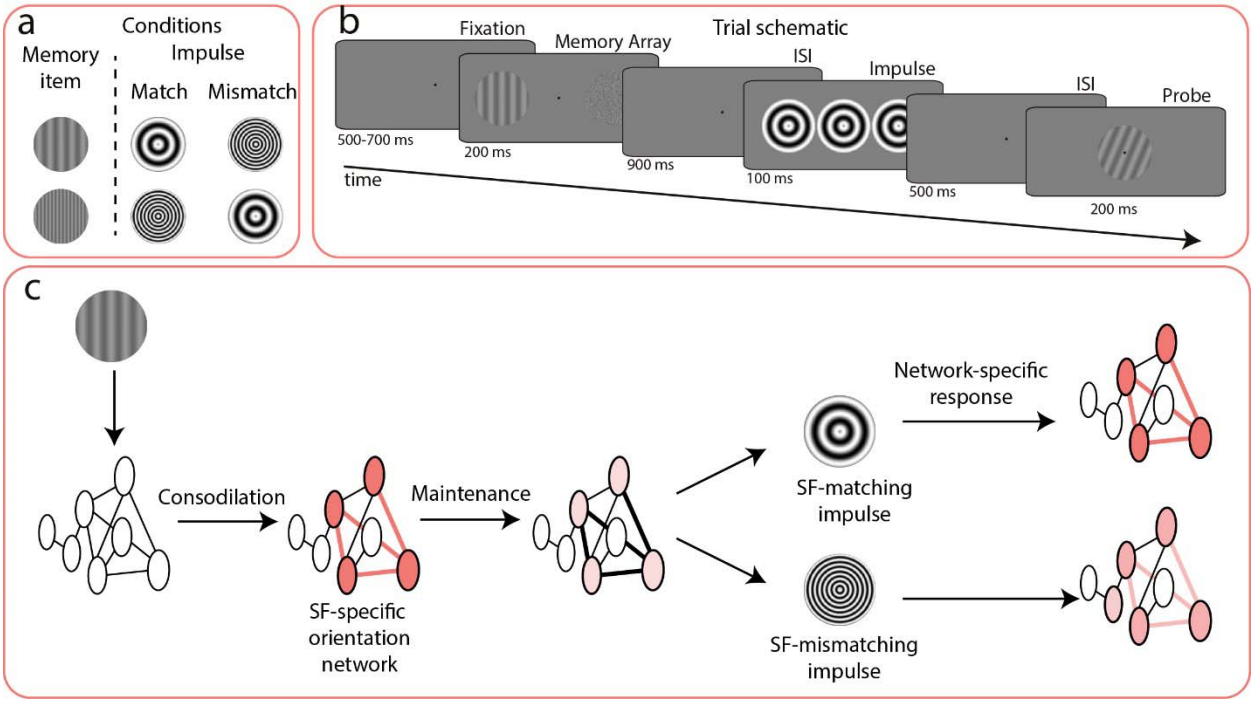

Figure 1. *Illustration of the trial schematic and hypothesis.* ***a.*** *Experimental manipulation showing memory item-impulse spatial frequency (SF) match and mismatch conditions.* ***b.*** *Trial schematic. Participants were asked to gaze at the center of the screen. After a variable delay period, the memory array, which consisted of a low or high spatial frequency orientation grating and a noise patch, were shown on either side of the fixation dot. The task was to remember the orientation, and judge whether it was clockwise or counterclockwise oriented relative to the probe. During the delay period, a visual impulse was shown. The spatial frequency of impulse either matched or did not match the orientation grating.* ***c.*** *Hypothesis. A matching visual impulse perturbs WM content better due to its shared spatial frequency-specific neural code.*

Method

Participants

A sample size of 30 was chosen following previous work using similar methodologies (Wolff et al., 2017; 2020a; 2020b). In total, 31 participants, most of whom were undergraduate students, participated at the University of Groningen in exchange for monetary compensation (8 euros per hour). One participant was excluded due to excessive EEG noise (more than 40% of the trials were contaminated). In the final sample, there were thus 30 participants (18 females [16 right-handed], 12 males [12 right-handed], mean age = 23.3, range = 16-32). All participants reported normal or corrected-to-normal vision and signed an informed consent form prior to participation. The study was conducted in accordance with the Declaration of Helsinki (2008).

Apparatus and stimuli

Participants were individually seated in dimly lit sound-attenuated testing cabins, approximately 60 cm from a 27-inch Asus IPS monitor (model VG279QM). The resolution was set to 1920 by 1080 pixels, at 16-bit color depth with a 100 Hz refresh rate. OpenSesame 3.2.8 (Mathôt et al., 2012) with the Psychopy back-end (Pierce et al., 2019) was used for trial preparation and data collection, running under the Microsoft Windows 10 operating system. Responses were collected with a standard keyboard.

The stimuli were presented on a grey background (RGB = 128, 128, 128). A black fixation point (RGB = 0, 0, 0) was maintained in the center of the screen throughout the trial. Memory items and probes were gray sine-wave gratings presented at 20% contrast, with a

diameter of 5.93° of visual angle (Figure 2a). Spatial frequencies of the memory items, probes, and impulse stimuli were either 0.5 cycles/degree (low spatial frequency) or 1.4 cycles/degree (high spatial frequency), depending on the experimental condition (Figure 2b). Memory items (orientation gratings) were presented on the left or right side of the fixation dot, at an eccentricity of 5.93° of visual angle. A Gaussian noise patch was shown at the same location on the other side of the fixation dot, matching the contrast and overall luminance of the memory items. Orientations were randomly chosen from 144 possible unique angles separated evenly between 0° and 179° with 1.25° separation. The angle difference between the memory item and the probe was chosen from 12 possible unique values, ranging from -40° to 40° (±5°, ± 10°, ± 16°, ± 24°, ± 32°, ± 40°, as in Wolff et al., 2017). Impulse stimuli consisted of three adjacent bull's eyes presented at the center of the screen. Each bull's eye was the same size as the memory items and probes (i.e., a diameter of 5.93° of visual angle).

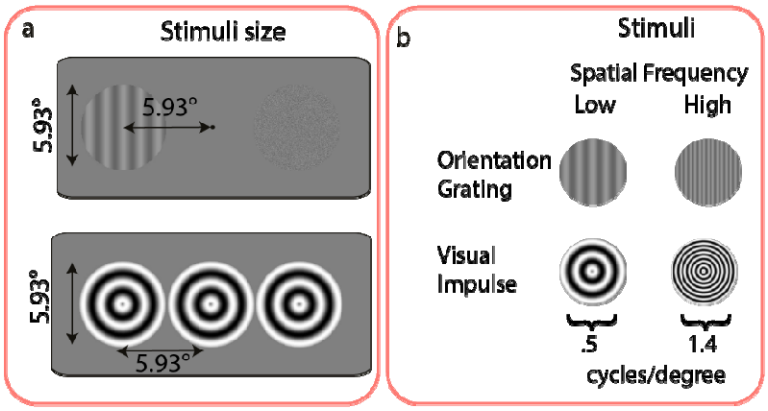

Figure 2. *Stimulus details in degrees of visual angle (°).* ***a****. Size and location of low and high spatial frequency memory items and impulses.* ***b.*** *Spatial frequencies of memory items and impulses.*

Procedure

Participants completed a visual working memory task (Figure 1b) while EEG was recorded. The task was to report whether the probe was rotated clockwise or counterclockwise relative to the memory item. Each trial began with a fixation cross with random temporal jitter, such that it was presented for 500-700 ms. Next, the memory item and Gaussian noise patch were simultaneously presented for 200 ms. After a 900 ms delay, the impulse stimulus was shown for 100 ms. After a 500 ms ISI, the memory probe was presented for 200 ms, and participants were required to give a speeded response by pressing m or c (counter-balanced between participants) within 1000 ms. Trial-wise feedback was provided for 200 ms (a happy smiley for the correct response and an unhappy smiley for the incorrect response). There was a 500 ms inter-stimulus interval between trials. Participants started the experiment with 64 practice trials. If they failed to perform above 60% accuracy, they were asked to redo the practice trials of the experiment. Participants were given a chance to have a break between each block and each session (see below). After each block, the average accuracy that the participant had achieved within was shown. The total duration of the study was four hours, including EEG capping.

Design

The principal variables of interest were whether the spatial frequency of the memory item matched that of the impulse and/or that of the probe (Figure 1c). The design was nevertheless also randomized and counterbalanced for the location of the memory item (left or right), the spatial frequency of the memory item (low or high), the spatial frequency of the impulse stimulus (low or high), and the spatial frequency of the probe stimulus (low or high). For each of the 16 resulting design cells, 144 unique orientations were shown. In addition, each probe difference was randomly assigned to those 144 unique orientations, which was counterbalanced within and

between cells. Therefore, there were 2304 trials in total (16 * 144), which were separated into four consecutive sessions. Each session (576 trials) consisted of 24 blocks, and each block consisted of 24 trials. After randomization for these 2304 trials was done for each participant, the trial order was shuffled and separated into four sessions. The randomization of stimuli and conditions was achieved with experimental code written in R 4.0 (R Core Team, 2020).

Behavioral data analysis

Mean accuracy was calculated for each participant across all trials for each condition of interest. To visualize the proportion of clockwise responses, counterclockwise responses were reverse-signed when the probe was counterclockwise relative to the memory item. Reaction time was analyzed similarly, but trials in which no response, a response that was too fast (<150 ms), or an incorrect response were given were discarded from the analysis.

EEG acquisition

The EEG signal was acquired from 64 Ag/AgCI electrodes and one external EOG electrode using an equidistant hexagonal layout. The ground electrode was placed on the participants' upper back. Electrodes placed above and below the left eye (EOG and 1L) and the temples (1LD and 1RD) were used for bipolar electrooculography. The impedance of all electrodes was kept below 10 kΩ. The signal was recorded at 1000 Hz using an ANT Neuro Eego Mylab amplifier and the associated software. During recording, the EEG was referenced to the electrode 5Z, and no filtering was applied.

EEG preprocessing

Using EEGLAB 2021 (Delorme & Makeig, 2004), the EEG signal was re-referenced to the common average of all electrodes and downsampled to 500 Hz. A high-pass filter of 0.1 Hz and a low-pass filter of 40 Hz were applied to the EEG signal. Noisy EEG channels were interpolated with the *pop_interp* function of EEGLAB. As a result, in four participants' one to five EEG channels were replaced through spherical interpolation. Data were epoched relative to impulse onset (-1550 ms to 2000 ms). Following that, independent component analysis was run to remove eye-movement-related (blinks and saccades) components from the EEG signal. Trials with other EEG artefacts were detected semi-automatically using the *ft_rejectvisual* function of Fieldtrip 2017 (Oostenveld et al., 2011), and excluded from all subsequent analyses.

Wolff and colleagues' (2020b) methodology was used for preprocessing EEG data for distance-based multivariate pattern analysis (MVPA). For the time-course decoding analysis, a sliding window approach was used, since pooling information over time may improve decoding accuracy (Grootswagers et al., 2017; Nemrodov et al., 2018). EEG data was downsampled to 100 Hz by taking the average of every 10 ms. Next, the data for each channel were normalized by subtracting the average voltage values within a sliding 100 ms time window from each voltage value (prior to each value), to remove stable activity that does not change within the entire time window. Therefore, only evoked dynamics were considered in this analysis.

As a secondary analysis, we pooled information over the entire pre-selected time window of interest. Following Wolff et al. (2020a; 2020b) we determined the time window of interest as 100 to 400 ms relative to the onset of stimulation (memory item, impulse). After downsampling the EEG data to 100 Hz, data was normalized by subtracting average voltage values within the time window of interest. This resulted in 30 values per channel, and each value was considered as a separate dimension (61 channels, excluding the bipolar EOG channels, by 30 values, 1830 in

total), which were used in the decoding analysis, resulting in a single decoding accuracy value per participant.

Orientation decoding

Following Wolff and colleagues (2020a; 2020b), Mahalanobis-distance-based MVPA was applied to decode memory item orientations. Although memory orientations were counterbalanced, given that a different number of trials were discarded from the EEG analysis due to artefacts, we used an 8-fold procedure with subsampling to equalize unbalanced orientation distributions between conditions. Trials were assigned to the closest of 16 variable orientation bins and randomly split into eight folds, seven of which constituted the train set, and one of them the test set. The number of trials in each orientation bin in each train set was equalized by random subsampling, matching the minimum number of trials in any orientation bin. Next, the covariance matrix was computed with the train sets (seven folds), using a shrinkage estimator (Ledoit & Wolf, 2003). The activity of each orientation bin in the subsampled train trials was averaged. The average bins of the train trials were convolved with a half cosine basis set raised to the 15th power in order to pool information across similar orientations (Myers et al., 2015). Finally, Mahalanobis distances of each trial in the test fold were computed relative to the averaged and basis-weighted angle bins. This resulted in 16 distances per test trial, which were mean centered. This procedure was repeated for all test and train fold combinations.

Because trials were subsampled, we repeated this procedure 100 times for each of eight different orientation spaces (0° to 168.75°, 1.40625° to 170.1563°, 2.8125° to 171.5625°, 4.2188° to 172.9688°, 5.625° to 174.375°, 7.0313° to 175.7813°, 8.4375° to 177.1875°, 9.8438°

to 178.5938°, each in steps of 11.25°). For each trial, we thus obtained 800 samples for each of the 16 Mahalanobis distances. Distances were averaged per trial, ordered with regard to the orientation difference, and sign-reversed, such that larger values reflect larger pattern-similarity between the test trial and the averaged orientation bin. The pattern similarity curve was summarized into a single decoding value by taking the cosine vector mean, such that a higher value reflects higher pattern similarity.

Spatial frequency decoding

The spatial EEG activity pattern between 100 to 400 ms after memory item and impulse onset was used in spatial frequency reconstruction. The approach was similar to that of orientation reconstruction. Since there were only two spatial frequency conditions, the Mahalanobis distance of the spatial frequency condition relative to both spatial frequency conditions was computed. Following that, the Mahalanobis distance of the same spatial frequency condition was subtracted from that of the different spatial frequency condition. Positive values were converted to hits, and negative values were converted to misses. Hits and misses were averaged and presented as decoding accuracy.

Variance reduction analysis

EEG data were epoched from -200 to 500 ms relative to impulse onset. Trials were divided into two groups with regard to memory item – impulse spatial frequency pair conditions. Next, each EEG channel was averaged for each condition per participant, and the variance of each channel's activity was calculated on each time point of the EEG data. The variance of all

channels was averaged for each time point. Following that, we computed the relative change of variance using the following formula:

(data-base_data)/base_data

Where base_data was the variance during the baseline period (-200 to 0 ms relative to impulse onset) and data was the variance of the whole epoch.

The variance difference between match and mismatch conditions was calculated by subtracting one condition from another. A cluster-corrected permutation was run on the variance difference between conditions. Further, the average variance was estimated between 100 – 400 ms relative to impulse onset, since this time window was used for decoding memoranda. One extra participant was discarded from this analysis because the average variance in one condition was 2.5 standard deviations greater than that of the whole sample.

Alpha power reduction analysis

We also compared alpha power reduction between matching and mismatching impulses. Alpha power was first computed by filtering the voltage data of all EEG channels between 8 and 12 Hz and Hilbert transforming the result using the following code in Matlab:

abs(hilbert(eegfilt(data, hz, 8, 12)))

The filter length was 375 ms. The filtered data was subsequently averaged across all channels, before computing relative alpha power change after impulse presentation, using the same formula as for relative variance change ((data-base_data)/base_data)). Baseline alpha power was taken from the filtered data from -500 to -200 ms relative to impulse onset.

Event-related potentials

To assess whether there was any univariate change in the visual sensory evoked potential between impulse conditions, we examined the electrodes closest to the classic PO7 & PO8 scalp location (5LC & 5RC). EEG was epoched from -200 to 500 ms relative to impulse onset, followed by a baseline correction from -200 ms to 0 ms (presentation of impulse). Trial epochs were then averaged per subject and condition, per time point. The ERP difference between match and mismatch conditions was calculated by subtracting one condition from another.

Significance testing

A permutation T-test with 9999 Monte Carlo permutations was run for the analysis of behavioral data (response time and accuracy) using R (R Core Team., 2020), and decoding accuracy of pooled data using MATLAB. R was used to preprocess behavioral data and ggplot2 (Wickham, 2016) to plot outcomes. A cluster-corrected, one-sample permutation T-test with 100000 permutations was used for all time-course analyses. All tests were two-sided.

Results and discussion

Behavioral performance

As expected, accuracy increased, and RT decreased, as a function of the absolute difference between the orientation of the memory item and probe (Figure 3a-b). Average accuracy was 77.4%, with a standard deviation of 7.6%. Mean probe RT was 549.4 ms, with a standard deviation of 95.7 ms.

A marginally significant difference in accuracy existed between spatial frequency pairs of memory item and probe (p = .07; Figure 3c). Accuracy was 77.6% in the match (sd = 7.6%), and 77.1% in the mismatch (sd = 7.7%) condition. Participants responded faster when the memory

item's spatial frequency matched with the probe (p = .007; Figure 3d). Response time was 548.3 ms (sd = 95.3 ms) in the match condition, and 551.6 ms in the mismatch condition (sd = 95.7 ms). This provides behavioral evidence that matching a feature between memorandum and probe stimulus facilitates WM readout, even when the matching feature dimension is behaviorally irrelevant.

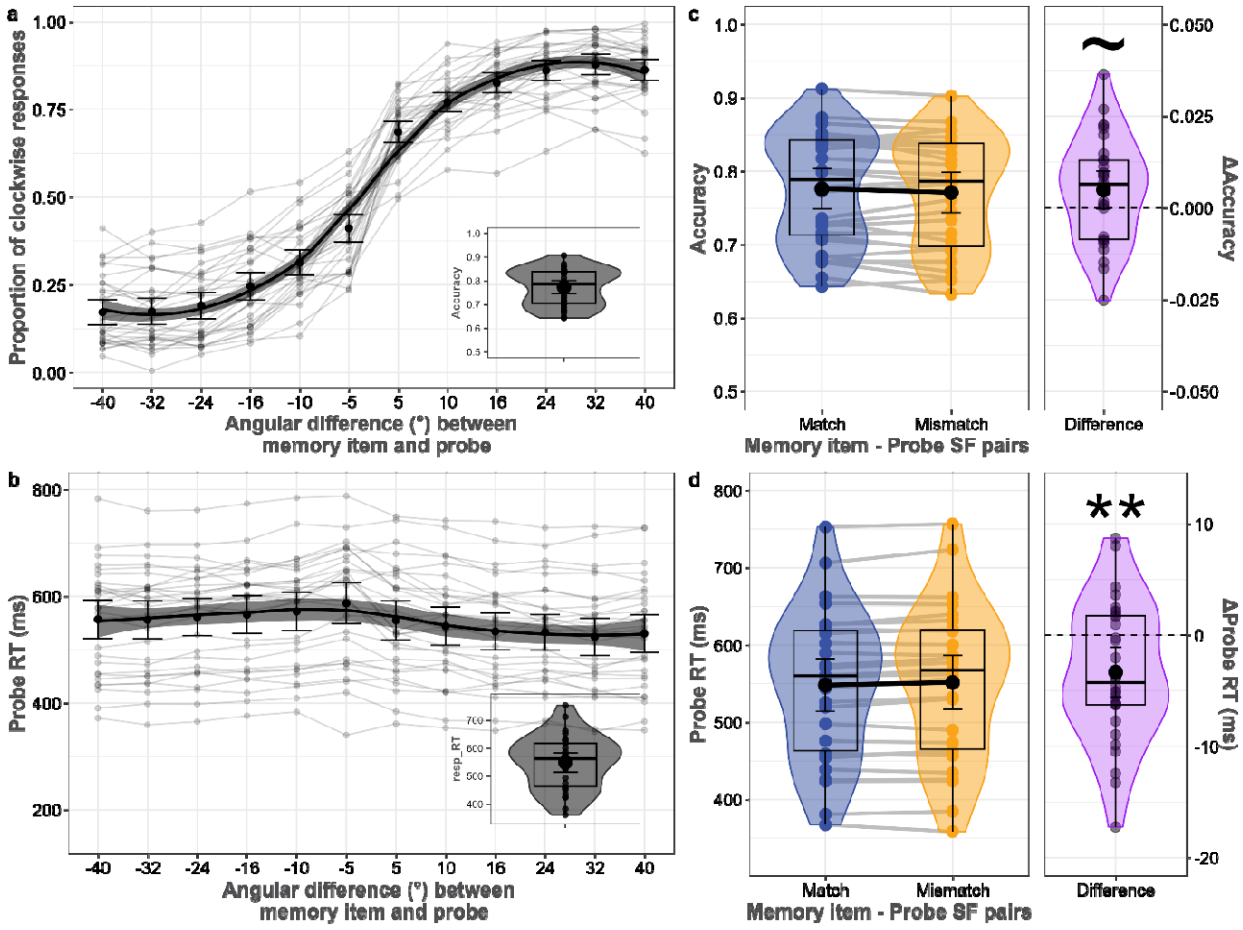

Figure 3. *Behavioral performance.* ***a****. The proportion of clockwise responses and* ***b.*** *probe response time as a function of the angular difference between the memory item and probe. The inset plot on the top panel shows average accuracy, and the bottom panel shows average probe response time.* ***c.*** *Mean accuracy of memory item and probe spatial frequency pairs.* ***d.*** *Probe response time of memory item and probe spatial frequency pairs. Colored and grey dots*

*represent individual data, black dots reflect averages, and error bars represent 95% confidence intervals calculated as 1.96 times the standard error of the mean. Transparent lines match subjects. Whisker plots show median and quartile values, and violin plots show the distribution. ~ shows p < .1, * shows p < .05, ** shows p < .01, and *** shows p < .001 (permutation tests).*

Decoding memory item orientation in match and mismatch conditions

Cluster-corrected permutation tests showed significant clusters of memory item orientation decoding during the encoding period, in both the match (76 – 488 ms, $p < .0001$; Figure 4a-b left panel) and mismatch conditions (56 – 548 ms, $p < .0001$). Confirming the obvious fact that the memory item - impulse spatial frequency pairs can only influence decoding accuracies after impulse onset, there were no differences between conditions at any time point before impulse onset ($p > .65$ at all time points). The analysis on the whole time window of interest (100 to 400 ms) showed significant decoding for both the match and mismatch condition ($p < .0001$; $p < .0001$, respectively; Figure 4c top panel), with no difference between them ($p = .216$).

Time course decoding after impulse onset showed a significant cluster for the match condition (154 – 374 ms, $p = .001$; Figure 4a-b right panel), as well as a significant difference between match and mismatch conditions (278 – 398 ms, $p = .01$). The mismatch condition failed to reach significance. The spatio-temporal analysis on the whole time window of interest (100 to 400 ms) nevertheless showed significant decoding for both the match and mismatch condition ($p < .001$; $p = .038$, respectively; Figure 4c bottom panel), as well as a significant difference between them ($p = .04$). These results provide evidence that the neural impulse response is WM-specific.

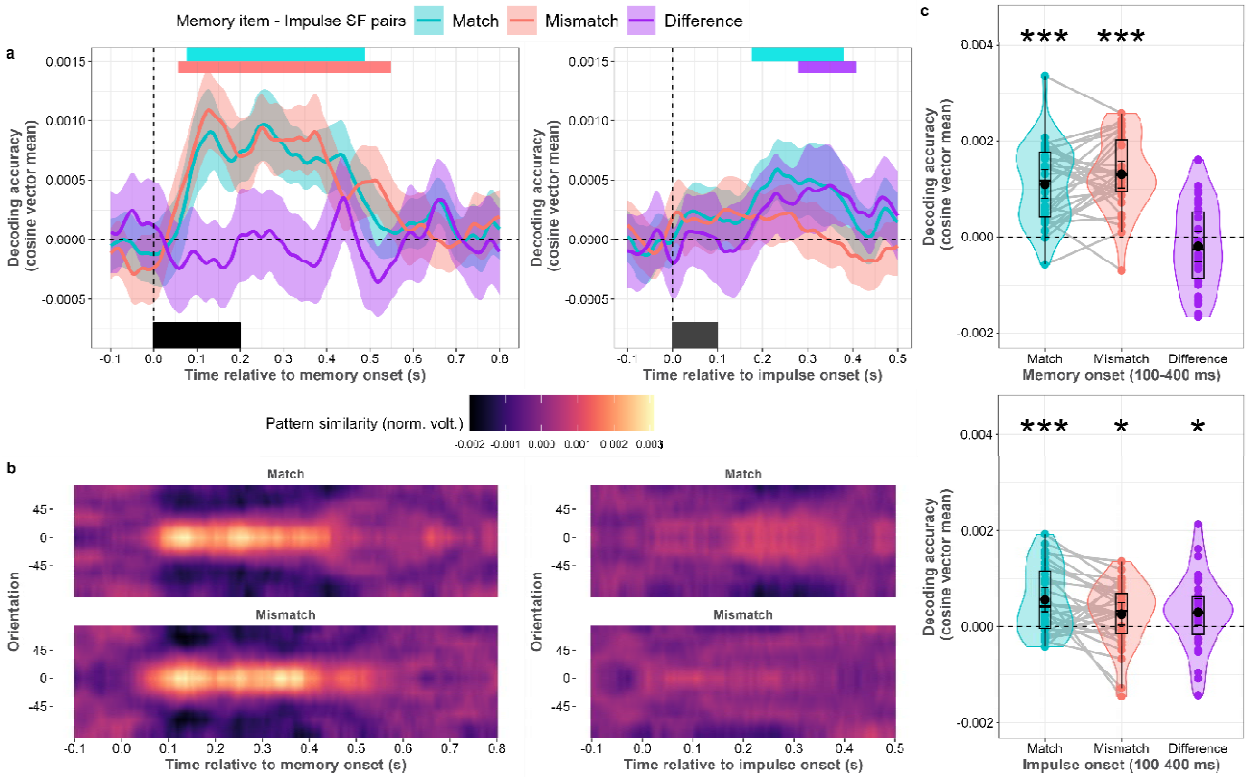

Figure 4. *Orientation decoding of memory item – impulse spatial frequency (SF) pairs, during encoding and maintenance.* ***a.*** *Normalized average pattern similarity (mean-centered, sign-reversed Mahalanobis distance) of the neural dynamics at each time point for both conditions during encoding (post-memory item presentation; left plot), and during maintenance (post-impulse presentation; right plot). Colored horizontal bars indicate significant clusters of orientation decoding. The black rectangles show the onset and offset of the memory item or impulse stimulus* ***b.*** *Average distance to template of all angle bins (mean-centered, sign-reversed Mahalanobis distance) of the neural dynamics at each time point for each condition after memory item presentation, and impulse presentation.* ***c.*** *Orientation decoding relative to memory onset, and impulse onset in the time window of interest (100 – 400 ms relative to onset). Boxplots, violin plots, dots, lines, error bars, and asterisks follow Figure 3.*

Testing for potential multivariate and univariate differences between memory item–impulse spatial frequency pairs

We were interested if there were any global differences between matching and mismatching impulse stimuli that might be related to the increased decoding of matching impulse trials. To this end, we compared several univariate measures of known stimulus-evoked neural responses between matching and mismatching impulses, such as event-related potentials, across-trial variance reduction, and alpha power reduction, which are all related to one another (e.g., Arazi et al. 2017; Wolff et al. 2021).

There were no statistically significant differences in event-related potentials as measured from electrodes closest to the conventional PO7 and PO8 scalp locations (5LC and 5RC; $p = 1$, Figure 5a). There were also no statistical differences in relative variance reduction ($p = 1$ at all time points, Figure 5b), nor in relative alpha power reduction ($p > .163$ at all time points, Figure 5c). Impulse presentation reduced variance and alpha power in both match and mismatch conditions after impulse offset. Relative variance change after impulse onset was significant between 2 – 124 ms and 222 – 476 ms in the match condition ($p = .046$ and $p = .007$, respectively; Figure 4b left panel), and between 94 – 500 ms in the mismatch condition ($p = .042$ and $p = .009$, respectively; Figure 5b left panel). Relative alpha power change after impulse onset was significant between 224 – 500 ms in the match condition, and between 226 – 500 ms in the mismatch condition ($p < .0001$, $p < .0001$, respectively; Figure 5c left panel).

Finally, we tested if there is a more subtle, multivariate difference between matching and mismatching impulse trials. While the time-course decoding showed no significant match/mismatch decoding ($p > .40$ at all time points, Figure 5d left panel), the time window of interest decoder did reach significance ($p = .016$, Figure 5d right panel). This suggests that there

are no global differences between matching and mismatching impulse stimuli that could explain the WM-content decoding difference reported above. We nevertheless found a subtle multivariate difference between matching conditions, suggesting that there may be unique neural signatures or patterns that are activated in the presence of matching versus mismatching impulses, without changing the global response amplitude.

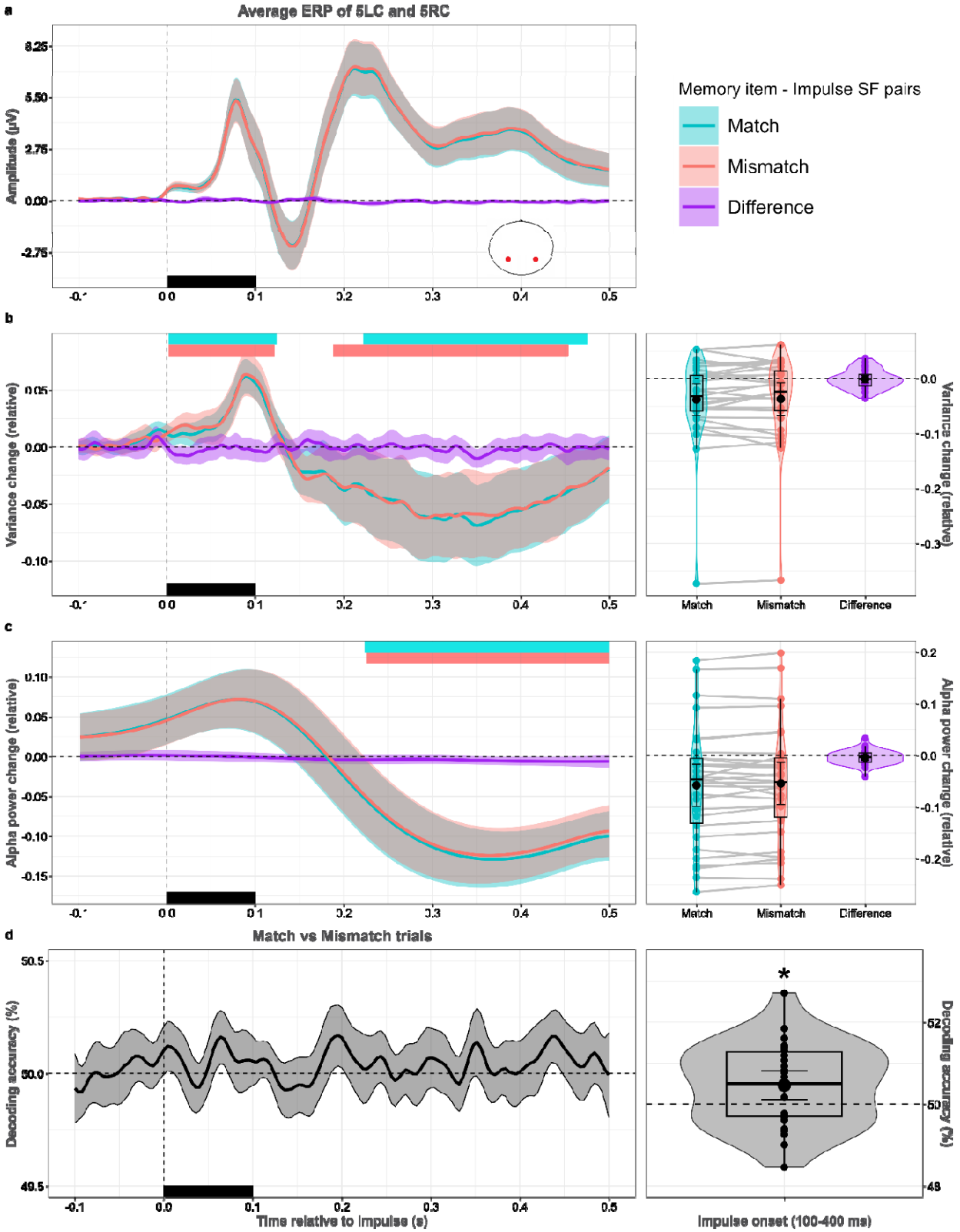
a
Average ERP of 5LC and 5RC
Amplitude (µV)
Memory item - Impulse SF pairs
Match
Mismatch
Difference
b
Variance change (relative)
Match
Mismatch
Difference
c
Alpha power change (relative)
Match
Mismatch
Difference
d
Match vs Mismatch trials
Decoding accuracy (%)
Time relative to impulse (s)
Impulse onset (100-400 ms)

Figure 5. *Univariate differences and condition decoding of match and mismatch trials.* ***a.*** *Impulse-locked event-related potentials in match and mismatch conditions.* ***b.*** *Left panel shows relative EEG variance for each time point. Right panel shows relative EEG variance change in the time window of interest (100 – 400 ms after impulse onset).* ***c.*** *Left panel shows relative alpha power change for each time point after impulse onset. Right panel shows relative alpha power change in the time window of interest.* ***d.*** *Left panel shows the decoding accuracy of experimental conditions (match vs. mismatch trials) per time point. Right panel shows the decoding accuracy of experimental conditions in the time window of interest. Colored rectangles on the top side of the left panels show significant clusters. Black rectangles show the onset and offset of the impulse.* *Colors, error bars, box plots, violin plots, dots, asterisks and lines follow Figure 3.*

Decoding memory item and impulse spatial frequency during encoding and maintenance

We tested whether the task-irrelevant spatial frequency of the memory item can be decoded during WM encoding and maintenance. The memory item's spatial frequency was significantly decodable during WM encoding ($p < .0001$; Figure 6a). During WM maintenance, decoding of both the spatial frequency of the memory item and that of the impulse was also significant ($p = .001$, $p < .0001$, respectively; Figure 6b).

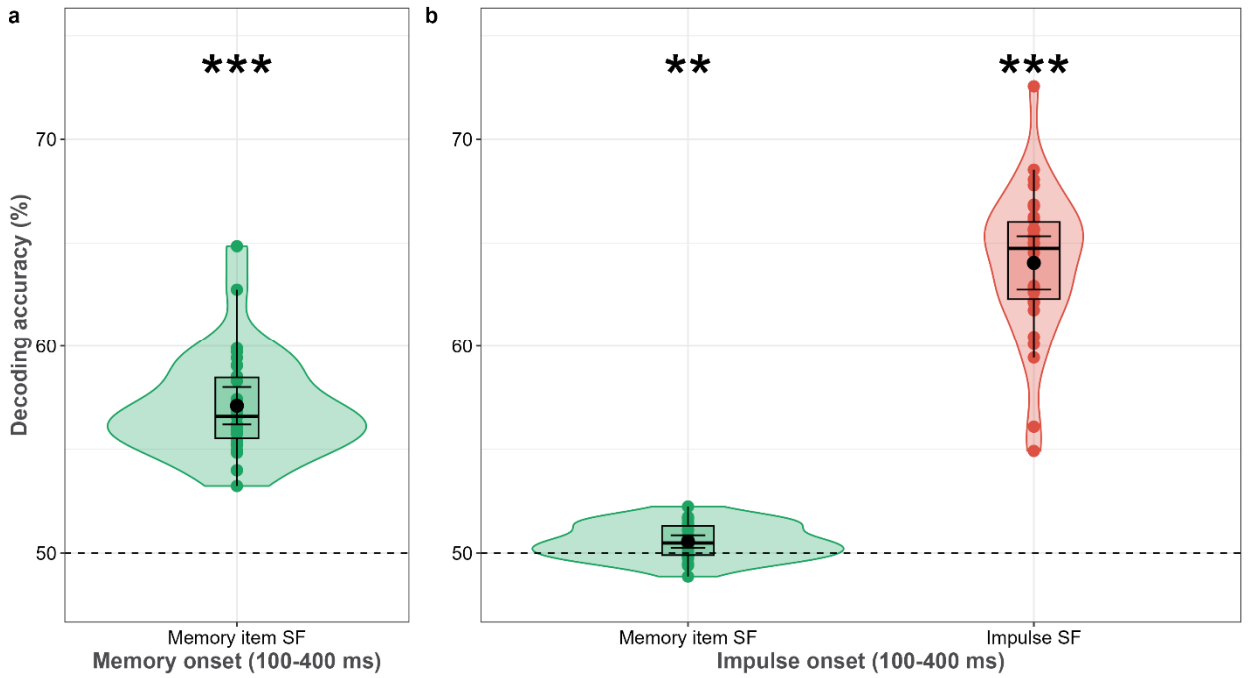

Figure 6. *Decoding accuracy (%) of the memory item and impulse spatial frequency (SF) during* ***a.*** *encoding and* ***b.*** *maintenance. Boxplots, violin plots, dots, error bars, and asterisks follow Figure 3.*

Decoding the location of the memory item during encoding and maintenance

Our final analysis tested whether the task-irrelevant spatial location of the memory item can be decoded during WM encoding and maintenance. Permutation T-tests showed that the location of the memory item was significantly decodable during WM encoding and maintenance (*p*s < .001; Figure 7). This finding was consistent with the decoding of SF that we also found, and suggests that all features of the memory items, task-irrelevant or not, were maintained in WM.

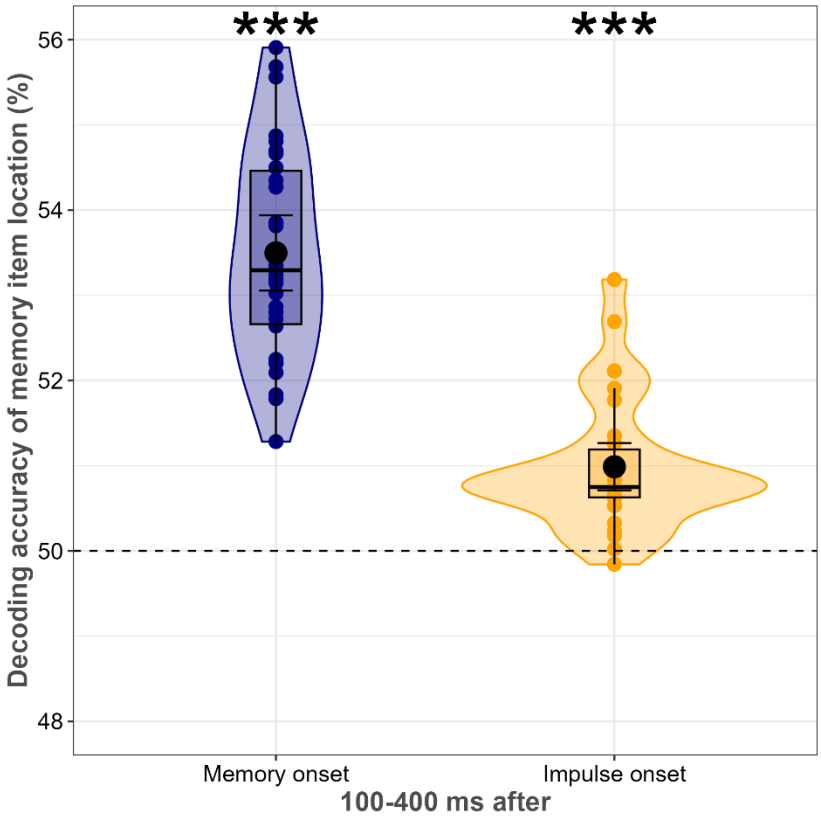

Figure 7. *Decoding accuracy (%) of the memory item location during WM encoding and maintenance. Boxplots, violin plots, dots, error bars, and asterisks follow Figure 3.*

Discussion

By either matching or mismatching the task-irrelevant feature of spatial frequency between memory item and impulse stimulus, we aimed to manipulate the degree to which the neural impulse response is patterned by the WM-specific neural trace. We found that matching the spatial frequency resulted in higher decoding accuracy of the memorized orientations, the task-relevant feature. This feature-specificity of the neural impulse stimulus provides evidence that its neural response reflects the stimulus-specific neural trace in WM (Stokes, 2015; Wolff et al., 2017). Thereby we confirmed one of the assumptions of activity-silent WM, which predicts that orientations are encoded and maintained in a spatially-specific and SF-specific network,

even if these features are irrelevant, due to the initial feed-forward sweep during visual processing that leaves behind the neural trace (Mongillo, 2008; Stokes, 2015).

We did not find univariate differences between matching and mismatching impulse stimuli. This is also in line with the activity-silent WM framework, where the neural impulse response is patterned by the WM network, depending on the degree that it interacts with it, without necessarily changing its absolute activation level (Figure 1c). It has previously been found that neural responses to stimuli that match visual WM content are increased (Awh et al., 2000; Gayet et al., 2017). However, in these studies, the matching visual features were task-relevant and likely maintained in an active neural code that biases attention towards the preferential processing of matching stimuli (Soto et al., 2008). Spatial frequency was task-irrelevant in our study, and unlikely to have been actively maintained. We believe that the increased WM decoding for matching impulse stimuli that we found is therefore unrelated to the attentional modulation of perception, which is why we did not observe an increase in neural response magnitude for matching impulses.

The present pattern of results speaks against a global, WM-unspecific impulse response, as has previously been proposed (Barbosa et al., 2021), and confirms the validity of the impulse perturbation approach, which is grounded in the assumption that it directly perturbs the WM-network, resulting in a WM-specific impulse response. If the impulse response had not been found to be WM-specific, this would have entailed that impulse perturbation can only access representations held in persistent-activity states, much like traditional methods. However, the presently observed increased WM-content decoding of a matching impulse can only be explained by a content-specific interaction between the impulse and the current, potentially activity-silent, state of the WM network.

We also observed that if the spatial frequency of the probe stimulus matched that of the memory item, behavioral performance improved. This can be explained by a more pronounced matched-filter response for matching stimuli, resulting in a quicker transition into the behaviorally relevant neural response that discriminates relative probe rotation (Myers et al., 2015; Sugase et al., 2008). This highlights that the WM-specificity of the impulse response reported here and previously (e.g., Fan et al., 2021; Kandemir & Akyürek, 2023; Wolff et al., 2017), should not be considered an epiphenomenon of WM-maintenance, but a useful neural mechanism for a task-specific WM-trace that is optimized for efficient readout (Myers, 2022; Nairne, 2002).

Furthermore, despite its behavioral irrelevance, spatial frequency and location of the memory were decodable from the impulse response, suggesting that it was more than a coincidental co-activator of the relevant orientation feature, but also a part of the memory trace itself (but see also Serences et al., 2009; Yu & Shim, 2017). This outcome is compatible with the idea that multiple features can be part of an object in memory, and that they can be encoded at minimal capacity costs (Luck & Vogel, 1997). It must be noted that in our case these multiple features shared basic, common encoding at the same location, so that the present 'object benefits' (i.e., the decoding of SF and location at impulse, and the reduced response times for matching probes), presumably had a stimulus-driven origin, rather than a higher-level one (cf. Balta et al., 2023). In other words, feature decoding might have been driven by their spatial integration, without necessarily requiring more conceptual object representations.

This outcome diverges from neural studies that showed little to no decoding for non-spatial task-irrelevant features during WM maintenance (Bocincova & Johnson, 2019; Yu & Shim, 2017). The divergence between our research and neural studies may have resulted from

methodological differences. First, the duration of the delay period may have contributed to the above chance-level decoding of task-irrelevant features during the delay period in our study, since the neural representations of task-irrelevant features are suggested to be transient. Thus, these features may disappear if the delay is long (Xu, 2010). Second, task-irrelevant features may not be at the center of attention during the delay period, and therefore their representations may not be maintained with sustained activity. This would make such representations difficult if not impossible to decode in fMRI and EEG without perturbation methods. Indeed, this pattern of results might suggest that irrelevant features are not maintained with sustained neural activity, and that short-term synaptic connectivity may be the mechanism. Third, the nature of the task-irrelevant feature may explain the divergence as spatial task-irrelevant features (i.e., location) have been decoded previously during the WM delay (Foster et al., 2017; Zhou et al., 2022), while task-irrelevant color and orientation have not been (Bocincova & Johnson, 2019; Yu & Shim, 2017). Therefore, it could be that SF plays a special role in WM, similar to location.

Our results are in line not only with predictions derived from the activity-silent WM framework, but also with the idea of sensory recruitment (Emrich et al., 2013; Pasternak & Greenlee, 2005; Postle, 2006), which suggests that WM content is maintained in the sensory areas that process and represent their constituent features (e.g., line orientation in primary visual cortex). The involvement of sensory brain regions in WM is usually tested by decoding the delay activity, which can lead to mixed results (Xu, 2018). By measuring the bottom-up neural impulse response we can probe sensory cortex without relying on measurable delay activity. Since visual cortex is known to process information at different spatial frequencies, the memory items in our task should have been processed and represented by the subpopulation of neurons in visual cortex that is tuned to their specific spatial frequency. During WM maintenance, within that

same population, stimulation that perturbs this network most strongly is likely to elicit the strongest memory-specific response. This is indeed what we found, which suggests that the orientation columns that process visual information also maintain it.

Conclusion

We found that matching a task-irrelevant stimulus feature between the WM-item and an irrelevant impulse stimulus presented during WM maintenance increased the WM-specific neural response, without changing its global response amplitude. Similarly, a matching probe stimulus increased WM recall as measured from a reduction in reaction times. These results suggest that the WM network maintains a stimulus-specific trace that can be targeted and read-out directly via external stimulation, as predicted by the activity-silent WM framework.

Data availability statement

Raw and processed EEG and behavioral data as well as analysis scripts will be available publicly upon publication of the manuscript on https://osf.io/7wrjh/.

Acknowledgments

This research was in part funded by an Open Research Area grant to EGA (NWO 464.18.114).

References

Arazi, A., Gonen-Yaacovi, G., & Dinstein, I. (2017). The magnitude of trial-by-trial neural variability is reproducible over time and across tasks in humans. *eNeuro, 4*(6). https://doi.org/10.1523/eneuro.0292-17.2017

Awh, E., Anllo-Vento, L., & Hillyard, S. A. (2000). The role of spatial selective attention in working memory for locations: Evidence from event-related potentials. *Journal of Cognitive Neuroscience, 12*(5), 840–847. https://doi.org/10.1162/089892900562444

Balta, G., Kandemir, G., & Akyürek, E. G. (2022). Object-based visual working memory: an object benefit for equidistant memory items presented within simple contours. *Psychological Research, 87*(5), 1569–1589. https://doi.org/10.1007/s00426-022-01757-w

Barbosa, J., Lozano-Soldevilla, D., & Compte, A. (2021). Pinging the brain with visual impulses reveals electrically active, not activity-silent, working memories. *PLOS Biology, 19*(10), e3001436. https://doi.org/10.1371/journal.pbio.3001436

Bocincova, A., & Johnson, J. S. (2019). The time course of encoding and maintenance of task-relevant versus irrelevant object features in working memory. *Cortex, 111*, 196–209. https://doi.org/10.1016/j.cortex.2018.10.013

Churchland, M. M., Yu, B. M., Cunningham, J. P., Sugrue, L. P., Cohen, M. R., Corrado, G. S., Newsome, W. T., Clark, A. M., Hosseini, P., Scott, B. B., Bradley, D. C., Smith, M. A., Kohn, A., Movshon, J. A., Armstrong, K. M., Moore, T., Chang, S. W., Snyder, L. H., Lisberger, S. G., . . . Shenoy, K. V. (2010). Stimulus onset quenches neural variability: A widespread cortical phenomenon. *Nature Neuroscience, 13*(3), 369–378. https://doi.org/10.1038/nn.2501

Curtis, C. E., & D'Esposito, M. (2003). Persistent activity in the prefrontal cortex during working memory. *Trends in Cognitive Sciences, 7*(9), 415–423. https://doi.org/10.1016/s1364-6613(03)00197-9

Delorme, A., & Makeig, S. (2004). EEGLAB: An open source toolbox for analysis of single-trial EEG dynamics including independent component analysis. *Journal of Neuroscience Methods, 134*(1), 9–21. https://doi.org/10.1016/j.jneumeth.2003.10.009

Duncan, D. H., van Moorselaar, D., & Theeuwes, J. (2023). Pinging the brain to reveal the hidden attentional priority map using encephalography. *Nature Communications, 14*(1), 4749. https://doi.org/10.1038/s41467-023-40405-8

Emrich, S. M., Riggall, A. C., LaRocque, J. J., & Postle, B. R. (2013). Distributed patterns of activity in sensory cortex reflect the precision of multiple items maintained in visual short-term memory. *The Journal of Neuroscience, 33*(15), 6516–6523. https://doi.org/10.1523/jneurosci.5732-12.2013

Fan, Y., Han, Q., Guo, S., & Luo, H. (2021). Distinct neural representations of content and ordinal structure in auditory sequence memory. *The Journal of Neuroscience, 41*(29), 6290–6303. https://doi.org/10.1523/jneurosci.0320-21.2021

Foster, J. J., Bsales, E. M., Jaffe, R. J., & Awh, E. (2017). Alpha-band activity reveals spontaneous representations of spatial position in visual working memory. *Current Biology, 27*(20), 3216-3223.e6. https://doi.org/10.1016/j.cub.2017.09.031

Funahashi, S., Bruce, C. J., & Goldman-Rakic, P. S. (1989). Mnemonic coding of visual space in the monkey's dorsolateral prefrontal cortex. *Journal of Neurophysiology, 61*(2), 331–349. https://doi.org/10.1152/jn.1989.61.2.331

Gayet, S., Guggenmos, M., Christophel, T. B., Haynes, J.-D., Paffen, C. L. E., Van der Stigchel, S., & Sterzer, P. (2017). Visual working memory enhances the neural response to matching visual input. *The Journal of Neuroscience*, *37*(28), 6638–6647. https://doi.org/10.1523/jneurosci.3418-16.2017

Kandemir, G., & Akyürek, E. G. (2023). Impulse perturbation reveals cross-modal access to sensory working memory through learned associations. *NeuroImage*, *274*, 120156. https://doi.org/10.1016/j.neuroimage.2023.120156

Kozachkov, L., Tauber, J., Lundqvist, M., Brincat, S. L., Slotine, J.-J., & Miller, E. K. (2022). Robust and brain-like working memory through short-term synaptic plasticity. *PLOS Computational Biology*, *18*(12), e1010776. https://doi.org/10.1371/journal.pcbi.1010776

Ledoit, O., & Wolf, M. N. (2003). Honey, I shrunk the sample covariance matrix. *SSRN Electronic Journal*. https://doi.org/10.2139/ssrn.433840

Lewis-Peacock, J. A., Drysdale, A. T., Oberauer, K., & Postle, B. R. (2012). Neural evidence for a distinction between short-term memory and the focus of attention. *Journal of Cognitive Neuroscience*, *24*(1), 61–79. https://doi.org/10.1162/jocn_a_00140

Lin, Y., Kong, G., & Fougnie, D. (2021). Object-based selection in visual working memory. *Psychonomic Bulletin & Review*, *28*(6), 1961–1971. https://doi.org/10.3758/s13423-021-01971-4

Luck, S. J., & Vogel, E. K. (1997). The capacity of visual working memory for features and conjunctions. *Nature*, *390*(6657), 279–281. https://doi.org/10.1038/36846

Lundqvist, M., Rose, J., Herman, P., Brincat, S. L., Buschman, T. J., & Miller, E. K. (2016). Gamma and beta bursts underlie working memory. *Neuron*, *90*(1), 152–164. https://doi.org/10.1016/j.neuron.2016.02.028

Lundqvist, M., Herman, P., & Miller, E. K. (2018). Working memory: Delay activity, yes! persistent activity? Maybe not. *The Journal of Neuroscience, 38*(32), 7013–7019. https://doi.org/10.1523/jneurosci.2485-17.2018

Masse, N. Y., Rosen, M. C., & Freedman, D. J. (2020). Reevaluating the role of persistent neural activity in short-term memory. *Trends in Cognitive Sciences, 24*(3), 242-258. https://doi.org/10.1016/j.tics.2019.12.014

Mathôt, S., Schreij, D., & Theeuwes, J. (2012). OpenSesame: An open-source, graphical experiment builder for the social sciences. *Behavior Research Methods, 44*(2), 314–324. https://doi.org/10.3758/s13428-011-0168-7

Miller, E. K., Lundqvist, M., & Bastos, A. M. (2018). Working memory 2.0. *Neuron, 100*(2), 463–475. https://doi.org/10.1016/j.neuron.2018.09.023

Mongillo, G., Barak, O., & Tsodyks, M. (2008). Synaptic theory of working memory. *Science, 319*(5869), 1543–1546. https://doi.org/10.1126/science.1150769

Myers, N. E. (2022). Considering readout to understand working memory. *Journal of Cognitive Neuroscience, 35*(1), 11–13. https://doi.org/10.1162/jocn_a_01921

Myers, N. E., Rohenkohl, G., Wyart, V., Woolrich, M. W., Nobre, A. C., & Stokes, M. G. (2015). Testing sensory evidence against mnemonic templates. *eLife, 4*. https://doi.org/10.7554/elife.09000

Nairne, J. S. (2002). The myth of the encoding-retrieval match. *Memory, 10*(5-6), 389–395. https://doi.org/10.1080/09658210244000216

Nemrodov, D., Niemeier, M., Patel, A., & Nestor, A. (2018). The neural dynamics of facial identity processing: insights from EEG-based pattern analysis and image reconstruction. *eNeuro, 5*(1). https://doi.org/10.1523/eneuro.0358-17.2018

Nikolić, D., Häusler, S., Singer, W., & Maass, W. (2009). Distributed fading memory for stimulus properties in the primary visual cortex. *PLoS Biology, 7*(12), e1000260. https://doi.org/10.1371/journal.pbio.1000260

Oostenveld, R., Fries, P., Maris, E., & Schoffelen, J. M. (2011). FieldTrip: Open source software for advanced analysis of MEG, EEG, and invasive electrophysiological data. *Computational Intelligence and Neuroscience*, 1–9. https://doi.org/10.1155/2011/156869

Pasternak, T., & Greenlee, M. W. (2005). Working memory in primate sensory systems. *Nature Reviews Neuroscience, 6*(2), 97–107. https://doi.org/10.1038/nrn1603

Pfurtscheller, G., Aranibar, A., & Maresch, H. (1979). Amplitude of evoked potentials and degree of event-related desynchronization (ERD) during photic stimulation. *Electroencephalography and Clinical Neurophysiology, 47*(1), 21–30. https://doi.org/10.1016/0013-4694(79)90029-4

Pfurtscheller, G., Neuper, C., & Mohl, W. (1994). Event-related desynchronization (ERD) during visual processing. *International Journal of Psychophysiology, 16*(2–3), 147–153. https://doi.org/10.1016/0167-8760(89)90041-x

Postle, B. R. (2006). Working memory as an emergent property of the mind and brain. *Neuroscience, 139*, 23–38. https://doi.org/10.1016/j.neuroscience.2005.06.005

R Core Team. (2020). *R: A language and environment for statistical computing. R Foundation for Statistical Computing*. Retrieved from http://www.R-project.org/

Remington, E. D., Narain, D., Hosseini, E. A., & Jazayeri, M. (2018). Flexible sensorimotor computations through rapid reconfiguration of cortical dynamics. *Neuron, 98*(5), 1005-1019.e5. https://doi.org/10.1016/j.neuron.2018.05.020

Rose, N. S., LaRocque, J. J., Riggall, A. C., Gosseries, O., Starrett, M. J., Meyering, E. E., & Postle, B. R. (2016). Reactivation of latent working memories with transcranial magnetic stimulation. *Science, 354*(6316), 1136–1139. https://doi.org/10.1126/science.aah7011

Schneegans, S., & Bays, P. M. (2017). Neural architecture for feature binding in visual working memory. *The Journal of Neuroscience, 37*(14), 3913–3925. https://doi.org/10.1523/jneurosci.3493-16.2017

Serences, J. T., Ester, E. F., Vogel, E. K., & Awh, E. (2009). Stimulus-specific delay activity in human primary visual cortex. *Psychological Science, 20*(2), 207–214. https://doi.org/10.1111/j.1467-9280.2009.02276.x

Shafi, M., Zhou, Y., Quintana, J., Chow, C., Fuster, J., & Bodner, M. (2007). Variability in neuronal activity in primate cortex during working memory tasks. *Neuroscience, 146*(3), 1082–1108. https://doi.org/10.1016/j.neuroscience.2006.12.072

Soto, D., Hodsoll, J., Rotshtein, P., & Humphreys, G. W. (2008). Automatic guidance of attention from working memory. *Trends in Cognitive Sciences, 12*(9), 342–348. https://doi.org/10.1016/j.tics.2008.05.007

Sprague, T. C., Ester, E. F., & Serences, J. T. (2016). Restoring latent visual working memory representations in human cortex. *Neuron, 91*(3), 694–707. https://doi.org/10.1016/j.neuron.2016.07.006

Sreenivasan, K. K., Curtis, C. E., & D'Esposito, M. (2014). Revisiting the role of persistent neural activity during working memory. *Trends in Cognitive Sciences, 18*(2), 82–89. https://doi.org/10.1016/j.tics.2013.12.001

Stokes, M. G. (2015). 'Activity-silent' working memory in prefrontal cortex: a dynamic coding framework. *Trends in Cognitive Sciences, 19*(7), 394–405. https://doi.org/10.1016/j.tics.2015.05.004

Stokes, M. G., Kusunoki, M., Sigala, N., Nili, H., Gaffan, D., & Duncan, J. (2013). Dynamic coding for cognitive control in prefrontal cortex. *Neuron, 78*(2), 364–375. https://doi.org/10.1016/j.neuron.2013.01.039

Stokes, M. G., Wolff, M. J., & Spaak, E. (2015). Decoding rich spatial information with high temporal resolution. *Trends in Cognitive Sciences, 19*(11), 636–638. https://doi.org/10.1016/j.tics.2015.08.016

Sugase-Miyamoto, Y., Liu, Z., Wiener, M. C., Optican, L. M., & Richmond, B. J. (2008). Short-term memory trace in rapidly adapting synapses of inferior temporal cortex. *PLoS Computational Biology, 4*(5), e1000073. https://doi.org/10.1371/journal.pcbi.1000073

Watanabe, K., & Funahashi, S. (2014). Neural mechanisms of dual-task interference and cognitive capacity limitation in the prefrontal cortex. *Nature Neuroscience, 17*(4), 601–611. https://doi.org/10.1038/nn.3667

Wickham, H. (2016). *Ggplot2: Elegant graphics for data analysis.* New York: Springer

Wolff, M. J., Akyürek, E. G., & Stokes, M. G. (2021). What is the functional role of delay-related alpha oscillations during working memory? *PsyArXiv*. https://doi.org/10.31234/osf.io/z6y5b

Wolff, M. J., Ding, J., Myers, N. E., & Stokes, M. G. (2015). Revealing hidden states in visual working memory using electroencephalography. *Frontiers in Systems Neuroscience, 9*. https://doi.org/10.3389/fnsys.2015.00123

Wolff, M. J., Jochim, J., Akyürek, E. G., & Stokes, M. G. (2017). Dynamic hidden states underlying working-memory-guided behavior. *Nature Neuroscience, 20*(6), 864–871. https://doi.org/10.1038/nn.4546

Wolff, M. J., Jochim, J., Akyürek, E. G., Buschman, T. J., & Stokes, M. G. (2020a). Drifting codes within a stable coding scheme for working memory. *PLOS Biology, 18*(3), e3000625. https://doi.org/10.1371/journal.pbio.3000625

Wolff, M. J., Kandemir, G., Stokes, M. G., & Akyürek, E. G. (2020b). Unimodal and bimodal access to sensory working memories by auditory and visual impulses. *The Journal of Neuroscience, 40*(3), 671–681. https://doi.org/10.1523/jneurosci.1194-19.2019

Xu, Y. (2010). The neural fate of task-irrelevant features in object-based processing. *The Journal of Neuroscience, 30*(42), 14020–14028. https://doi.org/10.1523/jneurosci.3011-10.2010

Xu, Y. (2018). Sensory cortex is nonessential in working memory storage. *Trends in Cognitive Sciences, 22*(3), 192–193. https://doi.org/10.1016/j.tics.2017.12.008

Zhou, Y., Curtis, C. E., Sreenivasan, K. K., & Fougnie, D. (2022). Common neural mechanisms control attention and working memory. *The Journal of Neuroscience, 42*(37), 7110–7120. https://doi.org/10.1523/jneurosci.0443-22.2022

Yu, Q., & Shim, W. M. (2017). Occipital, parietal, and frontal cortices selectively maintain task-relevant features of multi-feature objects in visual working memory. *NeuroImage, 157*, 97–107. https://doi.org/10.1016/j.neuroimage.2017.05.055